Time-gated total internal reflection fluorescence microscopy with a supercontinuum excitation source

Pierre Blandin, Sandrine Leveque-Fort, S. Lecart, C. Cossec, Marie-Claude Potier, Zsolt Lenkei, Frédéric Druon, Patrick Georges

Time-gated total internal reflection fluorescence microscopy with a supercontinuum excitation source

Pierre Blandin,[1,2,4] Sandrine Lévêque-Fort,[1,2,*] Sandrine Lécart,[2] Jack C. Cossec,[3] Marie-Claude Potier,[3] Zsolt Lenkei,[3] Frédéric Druon,[2,4] and Patrick Georges[2,4]

[1]Laboratoire de Photophysique Moléculaire, CNRS, Université Paris-Sud, Bat 210, 91405 Orsay, France

[2]Centre de Photonique Biomédicale, Centre Laser de l'Université Paris Sud, Université Paris-Sud, Bat 106, 91405 Orsay, France

[3]Laboratoire de Neurobiologie et Diversité Cellulaire, CNRS, Ecole Supérieure de Physique et de Chimie Industrielle, 75013 Paris, France

[4]Laboratoire Charles Fabry de l'Institut d'Optique, CNRS, Université Paris-Sud, Campus Polytechnique RD 128, 91127 Palaiseau cedex, France

*Corresponding author: sandrine.leveque-fort@u-psud.fr

Received 20 June 2008; revised 3 December 2008; accepted 4 December 2008; posted 5 December 2008 (Doc. ID 97630); published 14 January 2009

We present the instrumental development of a versatile total internal reflection fluorescence lifetime imaging microscopy setup illuminated by a supercontinuum laser source. It enables performing wide-field fluorescence lifetime imaging with subwavelength axial resolution for a large range of fluorophores. The short overall acquisition time and the axial resolution are well suited for dynamic neurobiological applications. © 2009 Optical Society of America

OCIS codes: 170.0180, 170.1530, 170.2520, 170.6920, 260.6970.

1. Introduction

For various biomedical applications, especially in the investigation of protein–protein interaction for signaling, activation, and inhibition phenomena, imaging with high spatial and temporal resolutions is required to study intracellular processes.

In neurobiology the subcellular neuronal localization of many proteins, such as type I cannabinoid receptor (CB1R) or amyloid-β precursor protein (APP), gives crucial information about their trafficking and the neuronal structure. In fact, previous results show that the localization profoundly modifies their production, activation, clearance, and aggregation [1,2]. It is thus necessary to develop highly resolved imaging methods in a physiologically relevant cellular context that allow both the localization of these proteins with subneuronal resolution and the parallel detection of their activity. Förster resonance energy transfer (FRET) is commonly used to follow protein activity and one of the techniques to measure FRET efficiency is to monitor the fluorescence lifetime of the FRET donor [3]. Moreover, as these processes are dynamic, the acquisition time necessary to perform lifetime measurements must be as short as possible. In order to fulfill these requirements, we have developed a setup combining total internal reflection fluorescence microscopy (TIRFM), fluorescence lifetime imaging microscopy (FLIM), and a supercontinuum excitation source. We describe this so-called total internal reflection fluorescence lifetime imaging microscopy (TIRFLIM) technique and then present preliminary results obtained with various transfections in human embryonic kidney (HEK-293) cell lines to validate the setup.

0003-6935/09/030553-07$15.00/0

2. Principle of Total Internal Reflection Fluorescence Lifetime Microscopy

TIRFM is a very efficient and precise optical tool to observe the events which occur at or just below the plasma–membrane interface. This technique combines the advantages of wide-field imaging with an excitation on a large area, reduced acquisition time, and subwavelength axial resolution [4]. It gives access to the first hundreds of nanometers of the sample with a low fluorescence background and then is useful to follow the membrane activity or adhesion processes [5,6]. Currently, this technique is the simplest to obtain subwavelength axial resolution at video rate. TIRFM was first performed thanks to a prism [7], but in the past few years, many commercial objectives with high numerical aperture (NA) have appeared and allowed easily performing TIRFM with simpler setups in the so-called "through the objective configuration" [8]. Such a setup is more user friendly, since the sample is positioned on the inverted microscope, just as in classical epifluorescence, without compromising the accessibility (in contrast to a prism configuration where the cells are typically embedded between coverslips). Cells can thus be observed directly in open chamber slides, allowing the user to easily add reaction products and monitor cellular response in live. Moreover, higher NA confers better resolution to this kind of setup. However, the range of possible incident angles, and subsequently the penetration depths one can obtain, are limited by the objective NA.

Since TIRFM is a wide-field microscopy technique, the fluorescence signal can be detected for a field of, typically, $10^4\ \mu m^2$ with CCD cameras, so the image of the sample is directly accessible in a single shot without scanning or computer processing. To preserve this single-shot, wide-field imaging capability, it seems relevant to measure fluorescence lifetime as well in the wide-field technique [9–11]. This FLIM measurement is achieved in the time domain thanks to a high rate imager (HRI). This imager is a very high-rate, gated intensifier that enables opening temporal gates of, typically, a few hundreds of picoseconds in width for different delays after the laser excitation pulse and so to acquire a stack of images along the decay. The images from the HRI are optically relayed to a CCD camera. Afterward , by processing the intensity profiles pixel by pixel, the fluorescence decay is measured. With this FLIM technique, one can choose the optimal algorithm to do lifetime measurements. The number of gates can be reduced (down to only two gates in the case of the rapid lifetime determination algorithm, or RLD [12]) according to the lifetime expected and the signal level. This procedure considerably decreases the acquisition time to few seconds, which is a crucial parameter in the investigation of dynamic processes and to avoid fluorophore photobleaching.

Such an association has only been successfully realized by Schnekenburger *et al.* in the prism configuration [13,14], but our setup presents simpler excitation and epidetection, thanks to a single high NA objective. Furthermore, to have a versatile setup compatible with a large range of fluorophores, we used a megahertz picosecond supercontinuum laser. This new generation of source is widely used for biophotonics [15–17]. First, the low repetition rate chosen enables the observation of the fluorescence decays of many fluorophores, including fluorophores with relatively long lifetimes (typically up to a few tens of nanoseconds). Second, the large portion of the visible spectrum covered by the source allows the use of fluorophores with various excitation wavelengths. Then the only adjustment required is to choose the filter corresponding to the absorption band of the fluorophore used. And since we develop a wide-field fluorescence microscopy setup based on the one-photon-absorption process (without nonlinear effects involved), pulses of a few tens of picoseconds are suitable to record these lifetimes.

3. TIRFLIM Experimental Setup

The source is a 15 MHz supercontinuum fiber laser (Fianium SC450). This new generation of laser sources gives, for the first time, access to the blue range of the visible spectrum, with a spectral density sufficient to efficiently excite fluorophores. The pulse width has been measured shorter than 15 ps and the spectrum is flat in decibels from 450 to 1800 nm, which is remarkable for a supercontinuum source. Moreover, lower wavelengths are also accessible with the SC450 source (but not guaranteed by the constructor). In particular, it is possible to excite fluorophores, such as cyan fluorescent protein (CFP), with wavelengths around 430 nm. However, since the supercontinuum (SC) generation is a highly nonlinear process, the spectral broadening strongly depends on the pulse energy. Consequently, minor variations in pulse width or in power of the seeding fiber oscillator have direct repercussions on the generation of very low wavelengths at the edge of the spectrum plateau (from 420 to 450 nm). Because of this instability, a long term variation (hour timescale) from 1 to 5 on the power can be observed in the bluest part of the SC. Then, in this extra spectral range not included in the source specifications, a measurement of the incident excitation power and an adjustable optical density (from 0 to 4) are required to overcome this variation.

To avoid reinjection at 1064 nm in the laser and to filter out the NIR and IR band of the supercontinuum source from the excitation light entering the microscope, two 400–900 nm dielectric mirrors (Thorlabs Broadband dielectric mirrors with E02 coating) are used (Fig. 1). The beam diameter is enlarged by a telescope to reach a diameter of around 4 cm. The spectral range for the excitation is optimally adjusted using a filter set. A lens permits focussing the excitation beam in the back focal plane of the objective. A rotating plane mirror is positioned just before to adjust the angle of the beam incident on the lens. Thanks to a screw with a differential

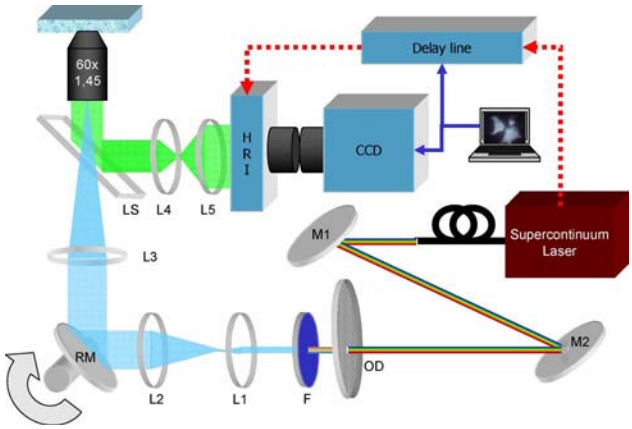

Fig. 1. (Color online) Experimental setup. M1, M2, plane broadband dielectric mirrors; OD, adjustable optical density; F, filter; L1, $f = 35$ mm; L2 and L3, $f = 300$ mm; RM, rotating plane mirror; LS, dichroic beam splitter; L4, $f = 50$ mm; L5, $f = 150$ mm; camera objectives, $f = 50$ mm.

micrometer head, the incident angle can be carefully controlled and estimated. It enables switching from classical wide-field illumination to a TIRF configuration and to evaluate the penetration depth of the evanescent wave. To perform TIRFM, an objective with 1.45 N. (Olympus TIRFM, 60×) is used.

For the detection part, a ×3 telescope enables properly relaying the images to the HRI. This HRI (Kentech Instrument Ltd.) can open gates from 200 ps to 1 ns wide with increments of 100 ps from gate to gate, or larger gates of 4.8 or 10 ns wide, essentially used for RLD acquisition. It is triggered to the laser via a delay line with increment spacing between gates down to 25 ps. The phosphor screen output of the HRI is imaged onto the CCD camera (Hamamatsu Orca AG), using 1:1 relay optics comprising two camera lenses mounted face to face (Fig. 1).

4. Setup Characterization

A. Spatial Resolution

To measure the lateral resolution of our setup, we observed fluorescent beads of subdiffraction diameters (100 nm excited at 580 nm and observed at 605 nm. By plotting the intensity profile, we measured a full width at half-maximum (FWHM) of 390 nm, corresponding approximately to 5 pixels on the CCD camera. The higher value in comparison to its theoretical limit confirms a little degradation of lateral resolution due to the phosphor screen of the HRI. This value also illustrates the role of the ×3 telescope, since a PSF is larger than 1 pixel.

Up to now, we are not able to measure accurately the penetration depth of the evanescent wave, which is directly linked to the axial resolution. Nevertheless, this value can be estimated by measuring the angle of the excitation beam incident on the lens before the microscope and calculating the penetration depth, given by

$$d = \frac{\lambda_{\mathrm{exc}}}{4\pi(n_1^2 \sin^2(\theta_{\mathrm{inc}}) - n_2^2)^{\frac{1}{2}}}, \quad (1)$$

where λ_{exc} is the excitation wavelength, n_1 and n_2 are the refraction indices of, respectively, the glass coverslip and the sample, and θ_{inc} is the incident angle of the excitation beam at the interface between the glass coverslip and the sample.

B. Validation of the Time-Gated Detection

We also tested the accuracy of our time-resolved detection. Since our first experiments were based on the determination of CFP lifetime in cells to highlight FRET, we chose appropriate detection parameters to permit this measurement in the best conditions and we made the validation with fluorophores that h have comparable fluorescence lifetimes.

After checking the parameter's influence on the lifetime measured, we decided to use large gates of 800 ps for the HRI, shutter times of 250 ms for the camera, and a 13 time-gated-images algorithm to have precise measurements while having enough signal with low excitation power (some hundreds of microwatts) and avoiding photobleaching. For each delay after the pulse (respectively 0, 350, 750, 1000, 1500, 2000, 2500, 3000, 4000, 5000, 6000, 8000, and 10,000 ps for our 13 time-gated-images algorithm), we averaged 10 images to obtain a time-gated image (2.5 s acquisition time). The overall acquisition time did not exceed 35 s.

First, we tested the repeatability of this time-resolved detection with stable sample of rhodamine B diluted in ethanol for two signal levels, one comparable with the one obtained with fluorophores in cells, the other at the sensibility limit of the HRI. The results showed a good reproducibility of the measure for the lifetime as well as for the standard deviation; for 20 successive measurements, we obtained a standard deviation of 2.7 and 4.1 ps and an average of around 2.3 ns in both cases for the averages of the 20 FLIM maps at, respectively, the fluorescence signal level and the low level.

Second, we compared the lifetimes measured with our setup to lifetimes obtained with a commercial two-photon absorption FLIM setup (Leica SP5 microscope associated with a Coherent Chameleon femtosecond laser and a Picoquant data acquisition card). Two well-known samples, with lifetimes comparable with CFP with or without FRET, were used: rhodamine B in ethanol and rhodamine B in water. We obtained the same values with the two setups. For the rhodamine B in ethanol and in water, respectively, we obtained an average of 2.22 and 1.79 ns with a standard deviation of 29 ps for both with our homemade setup. With the commercial setup, the values obtained were 2.23 and 1.79 ns with a standard deviation of 0.08 ns for an average of 1900 counts per pixel through the image.

Furthermore, with these ultrastable samples, we also tested the RLD technique. Since the lifetime

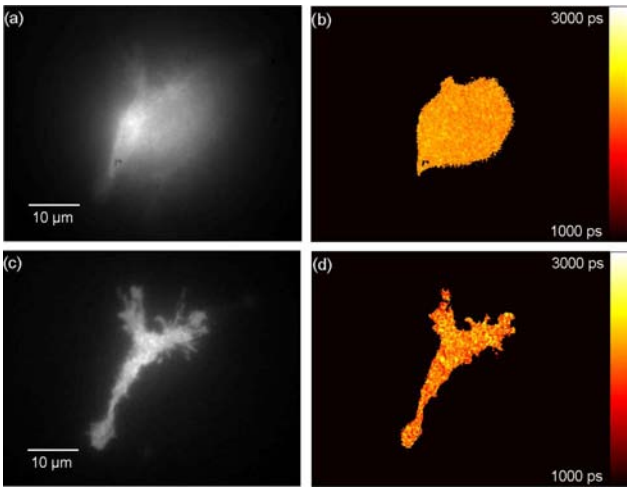

Fig. 2. (Color online) (a), (c) Intensity images and (b), (d)FLIM maps of a HEK-293 cell transfected with APP-CFP. Comparison of results obtained in (c), (d) TIRF and in (a), (b) classical epifluorescence. The average lifetimes for the entire cell obtained are (b) 2180 ± 68 ps and (d) 2100 ± 168 ps.

expected is around 2 ns, the gate width of 4.8 ns is approximately 2.5 times longer. In this range, the RLD algorithm with 50% overlapping for the two gates is preferable [18]. We opened two gates of 4.8 ns, the first one just after the excitation pulse and the second one 2.4 ns after the pulse. We obtained an average of 2.24 and 1.76 ns, with a standard deviation of 33 ps for both, for the rhodamine B in ethanol and in water, respectively. Lifetime can thus be determined using our time-gated TIRF setup with a similar resolution as that of using a TCSPC system [19] but with an RLD acquisition time considerably reduced to few seconds.

5. Multiple Color Living Cells Imaging

Thanks to the validation measurements set, the TIRFLIM setup was optimized for investigation of biological samples. We observed HEK-293 cells transfected with CFP-APP. HEK 293 cells are very easy to grow, transfect very readily, and possess some common characteristics with neuronal cells; that is why they are widely used in cell biology and especially in neurobiology research. To properly select excitation and emission wavelengths, a Semrock CFP/YFP FRET filter set was used (excitation, $\lambda = 438$ nm, $\Delta\lambda = 24$ nm; detection, $\lambda = 483$ nm, $\Delta\lambda = 32$ nm). The incident blue average power available on the sample was adjusted to around $450\,\mu$W and below to avoid photobleaching. In the TIRF configuration, we performed the measurements with an evanescent wave penetration depth estimated at between 160 and 190 nm. The depth estimation was obtained by using Eq. (1), with $\lambda_{\text{exc}} = 438$ nm, $n_1 = 1,50$, $n_2 = 1,38$, and θ_{inc} between 68 and 69 deg. The same multigates algorithm as in Subsection 4.B was used, with identical acquisition parameters.

To underline the gain in axial resolution of the TIRFLIM setup, we recorded intensity images and a FLIM map in classical epifluorescence and in TIRF for the same cell (Fig. 2). In TIRF, we obtained a better contrast. The excitation by an evanescent wave allowed us to get rid of the parasitic fluorescence signal from the cytoplasm. Only the plasma membrane and its close proximity was imaged. The FLIM maps of the CFP in epifluorescence and in TIRF are, respectively, reported in Figs. 2(b) and 2(d). The average lifetime obtained for the entire cell is 2180 ± 68 ps in epifluorescence and 2100 ± 168 ps in TIRF. The small difference in the average can be explained by the possible quenching of the fluorescence with the interface, which causes a shorter lifetime in

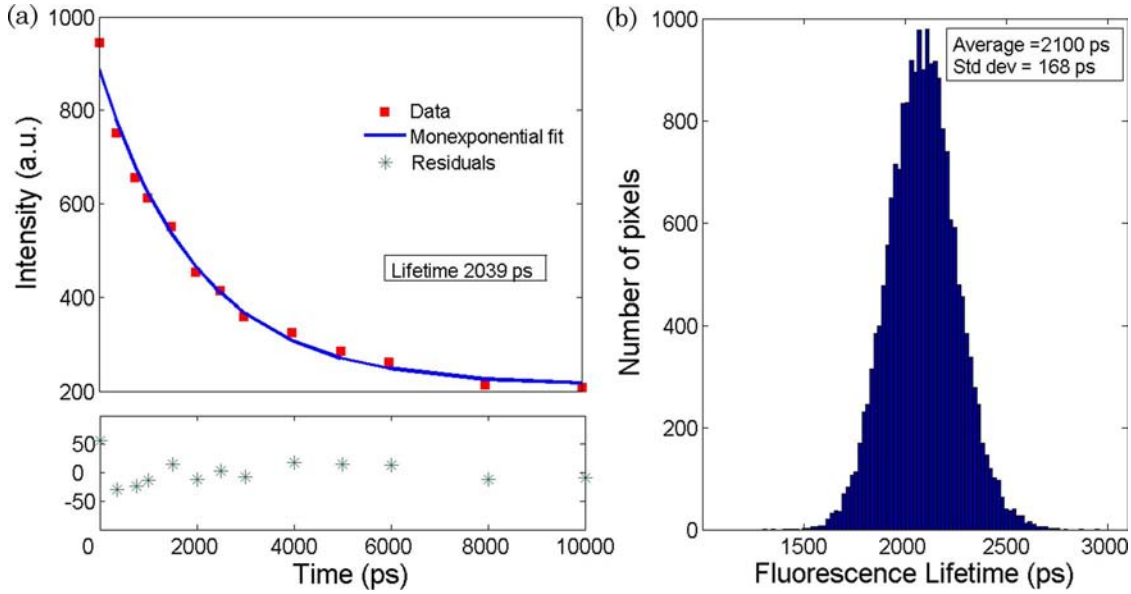

Fig. 3. (Color online) (a) Fluorescence decay for one pixel of the TIRFLIM map reported Fig. 2(d), fitted with a monoexponential model, and (b) histogram of the lifetimes calculated for the entire map.

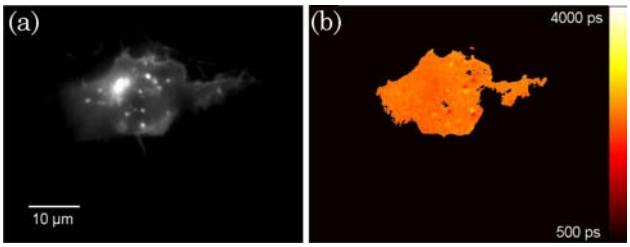

Fig. 4. (Color online) (a) TIRF intensity image and (b) TIRFLIM map of a HEK-293 cell expressing green fluorescent protein (GFP) tagged CB1 receptor. The average lifetime obtained is 2430 ± 100 ps.

TIRF. As expected, the standard deviation in epifluorescence is lower since the fluorescence signal collected is higher.

The histogram corresponding to the TIRFLIM map [Fig. 3(b)] shows a quite homogeneous distribution of the CFP fluorescence lifetime throughout the cell. Figure 3(a) shows typical fluorescence decay for one pixel; we can see a good agreement between the data set and the monoexponential decay model.

To demonstrate the large versatility of this setup, we realized different transfections of HEK cells with various fluorophores. With these examples, by selecting only accurate filters, we could demonstrate fluorophore excitation in the 438 to 531 nm range. But this excitation range can even be broader according to the SC source emission. On the one hand, we performed TIRFLIM in HEK cells expressing CB1R green fluorescent protein (GFP). For these measurements, we used our setup with a GFP set filter (excitation, $\lambda = 472$ nm, $\Delta\lambda = 30$ nm; detection: $\lambda = 520$ nm, $\Delta\lambda = 35$ nm). The incident average power on the sample was around $510\,\mu$W. We obtained an average lifetime of 2430 ± 100 ps (Fig. 4).

On the other hand, we observed HEK-293 cells but cotransfected them with APP yellow fluorescent protein (YFP) and CB1R-mCherry. For YFP (excitation, $\lambda = 482$ nm, $\Delta\lambda = 35$ nm; detection: $\lambda = 536$ nm, $\Delta\lambda = 40$ nm; incident power around $650\,\mu$W), we measured an average lifetime of 2592 ± 159 ps (Fig. 5). For mCherry (excitation, $\lambda = 531$ nm, $\Delta\lambda = 40$ nm; detection: $\lambda = 607$ nm, $\Delta\lambda = 36$ nm; incident power around $600\,\mu$W), an average value of 1358 ± 57 ps was obtained (Fig. 6). The standard deviations for these three measurements are quite different because the fluorescence signal collected depended on the fluorophore observed and on the position of the protein labeled in the cell. For all these measurements, the incident angle was the same and, consequently, the penetration depth changed only due to the wavelength. All these measurements are reported in Table 1. The values obtained with these different fluorophores are in good agreement with the lifetimes reported by other authors [19–21].

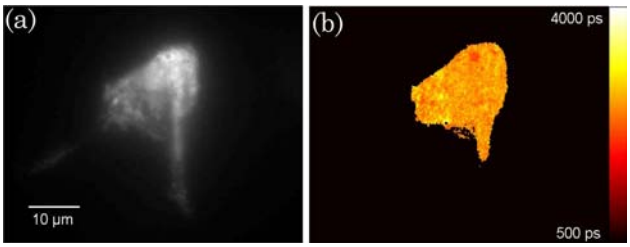

Fig. 5. (Color online) (a) TIRF intensity image and (b) TIRFLIM map of the YFP in a HEK-293 cell cotransfected with mCherry-CB1R and YFP-APP. The average lifetime obtained is 2592 ± 159 ps.

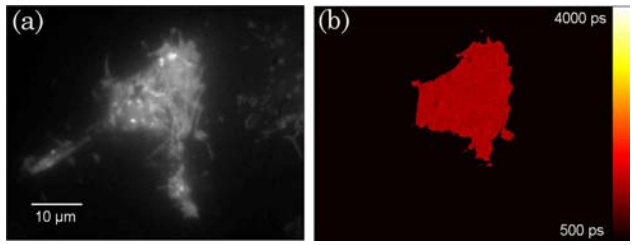

Fig. 6. (Color online) (a) TIRF intensity image and (b) TIRFLIM map of the mCherry in the same cell as Fig. 5. The average lifetime obtained is 1358 ± 57 ps.

6. Neurobiological Applications

Actually, the development of this setup was motivated by two neurobiological applications.

The first process under investigation is the activation of CB1Rs on the plasma membrane, leading to downregulation of cyclic adenosine monophosphate (cAMP) production in neurons. Our goal is to perform FRET-based detection of the mobilization of cAMP by using a new FRET-based probe, named AKAR [22]. The second biological process studied is the homodimerization of amyloid precursor protein (APP), a membrane protein involved in Alzheimer's disease [23]. We use APP labeled with CFP and with YFP. By transfecting HEK-293 cells with both, we will be able to observe the homodimerization of APP thanks to the subsequent FRET between CFP and YFP. To sum up, our global motivation is to highlight FRET between CFP and YFP in the plasma membrane.

We present here preliminary results obtained with a positive indicator of FRET between CFP and YFP transfected in HEK-293 cells. This FRET indicator is a molecular construction in which the two fluorophores are separated by 24 amino acids, leading to 80% of FRET through the entire sample. Thanks to TIRF, we imaged the indicators on or just below the plasma membrane. The results obtained show

Table 1. Results Obtained for Various Fluorophores Transfected in HEK-293 Cells[a]

Fluorophore	Excitation (nm)	Detection (nm)	Lifetime Measured (ps)	Standard Deviation (ps)
CFP	438	483	2100	168
GFP	472	520	2430	100
YFP	482	536	2592	159
mCherry	531	607	1358	57

[a]The different excitation peaks wavelengths are reported.

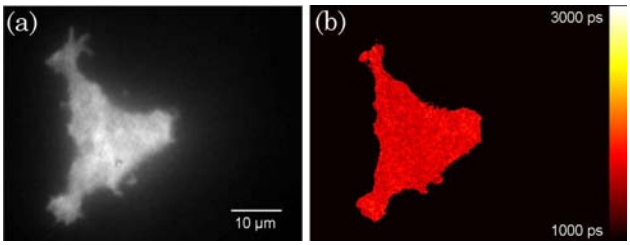

Fig. 7. (Color online) (a) TIRF intensity image and (b) TIRFLIM map of CFP in a HEK-293 cell transfected with a FRET indicator couple. The average lifetime obtained is 1650 ± 110 ps.

a lifetime 450 ps shorter than the one obtained with CFP alone. The lifetime is around 1650 ps with a standard deviation of 110 ps (Fig. 7). Regarding these results, we are confident in the capacity of our setup to measure even lower FRET efficiency between CFP and YFP in the plasma membrane.

7. Conclusion

We have presented the realization of a versatile TIRFLIM setup, which allows performing wide-field fluorescence lifetime imaging for a large range of fluorophores within a few seconds of acquisition. We presented the images obtained with HEK-293 cells transfected with CFP-APP, YFP-APP, mCherry-CB1R, and GFP-CB1R. We have also demonstrated the potential to measure FRET between CFP and YFP thanks to positive indicators. We are currently using this setup to tackle neurobiological issues and, in particular, we monitor FRET efficiency to identify biological processes at the membrane. The implementation of RLD detection for these applications will reduce the acquisition time to perform quasi real-time measurements. With the characteristics of the evanescent wave polarization [24], such a setup could also find applications in fluorescence anisotropy studies [25,26]. It would be useful as well for time-gated imaging of fluorophores with longer lifetimes, such as quantum dots [27].

The authors thank Vincent Studer for helpful discussions on this development. This research has been partially supported by the research program Pôle Laser from the Contrat Plan Etat Région (2000–2006) (French State and Conseil Général de l'Essonne), the Mission Ressources et Compétences Technologiques (MRCT) from the CNRS, and the Programme Pluri Formation (PPF) from the Université Paris-Sud.

References

1. C. Leterrier, J. Lainé, M. Darmon, H. Boudin, J. Rossier, and Z. Lenkei, "Constitutive activation drives compartment-selective endocytosis and axonal targeting of type 1 cannabinoid receptors," J. Neurosci. **26**, 3141–3153 (2006).
2. K. S. Vetrievel and G. Thinakaran, "Amyloidogenic processing of beta-amyloid precursor protein in intracellular compartments," Neurology **66**, S69–S73 (2006).
3. H. Wallrabe and A. Periasamy, "Imaging protein molecules using FRET and FLIM microscopy," Curr. Opin. Biotechnol. **16**, 19–27 (2005).
4. D. Axelrod, "Total internal reflection fluorescence microscopy in cell biology," Traffic **2**, 764–774 (2001).
5. N. Thompson and B. Lagerholm, "Total internal reflection fluorescence: applications in cellular biophysics," Curr. Opin. Biotechnol. **8**, 58–64 (1997).
6. J. Burmeister, L. Olivier, W. Reichert, and G. Truskey, "Application of total internal reflection fluorescence microscopy to study cell adhesion to biomaterials," Biomaterials **19**, 307–325 (1998).
7. D. Axelrod, "Cell-substrate contacts illuminated by total internal reflection fluorescence," J. Cell Biol. **89**, 141–145 (1981).
8. D. Axelrod, "Selective imaging of surface fluorescence with very high aperture microscope objectives," J Biomed. Opt. **6**, 6–13 (2001).
9. S. Leveque-Fort, D. Papadopoulos, S. Forget, F. Balembois, and P. Georges, "Fluorescence lifetime imaging with a low repetition rate passively mode-locked diode-pumped Nd:YVO4 oscillator," Opt. Lett. **30**, 168–170 (2005).
10. P. Herman, H. J. Lin, and J. R. Lakowicz, "Lifetime based imaging," in *Biomedical Photonics Handbook* (CRC Press, 2003).
11. J. Siegel, D. S. Elson, S. E. D. Webb, D. Parsons-Karavassilis, S. Lévêque-Fort, M. J. Cole, M. J. Lever, P. M. W. French, M. A. A. Neil, R. Juskaitis, L. O. Sucharov, and T. Wilson, "Whole-field five-dimensional fluorescence microscopy combining lifetime and spectral resolution with optical sectioning," Opt. Lett. **26**, 1338–1340 (2001).
12. I. Munro, J. McGinty, N. Galletly, J. Requejo-Isidro, P. M. P. Lanigan, D. S. Elson, C. Dunsby, M. A. A. Neil, M. J. Lever, G. W. H. Stamp, and P. M. W. French, "Toward the clinical application of time domain fluorescence lifetime imaging," J Biomed. Opt. **10**, 051403 (2005).
13. H. Schneckenburger, M. Wagner, M. Kretzschmar, W. Strauss, and R. Sailer, "Laser-assisted fluorescence microscopy for measuring cell membrane dynamics," Photochem. Photobiol. Sci. **3**, 817–822 (2004).
14. C. von Arnim, B. von Einem, P. Weber, M. Wagner, D. Schwanzar, R. Spoelgen, W. Strauss, and H. Schneckenburger, "Impact of cholesterol level upon APP and BACE proximity and APP cleavage," Biochem. Biophys. Res. Comm. **370**, 207–212 (2008).
15. H. Kano and H. Hamaguchi, "In-vivo multi-nonlinear optical imaging of a living cell using a supercontinuum light source generated from a photonic crystal fiber," Opt. Express **14**, 2798–2804 (2006).
16. J. Tada, T. Kono, A. Suda, H. Mizuno, A. Miyawaki, K. Midorikawa, and F. Kannari, "Adaptively controlled supercontinuum pulse from a microstructure fiber for two-photon excited fluorescence microscopy," Appl. Opt. **46**, 3023–3030 (2007).
17. E. Auksorius, B. Boruah, C. Dunsby, P. Lanigan, G. Kennedy, M. Neil, and P. French, "Stimulated emission depletion microscopy with a supercontinuum source and fluorescence lifetime imaging," Opt. Lett. **33**, 113–115 (2008).
18. K. K. Sharman, A. Periasamy, H. Ashworth, J. N. Demas, and N. H. Snow, "Error analysis of the rapid lifetime determination method for double-exponential decays and new windowing schemes," Anal. Chem. **71**, 947–952 (1999).
19. Y. Chen and A. Periasamy, "Characterization of two-photon excitation fluorescence lifetime imaging microscopy for protein localization," Microsc. Res. Tech. **63**, 72–80 (2004).
20. W. Becker, A. Bergmann, M. Hink, K. König, K. Benndorf, and C. Biskup, "Fluorescence lifetime imaging by time-correlated single-photon counting," Microsc. Res. Tech. **63**, 58–66 (2004).
21. E. Merzlyak, J. Goedhart, D. Shcherbo, M. Bulina, A. Shcheglov, A. Fradkov, A. Gaintzea, K. Lukyanov, S. Lukyanov, T. Gadella, and D. Chudakov, "Bright monomeric red fluorescent protein with an extended fluorescence lifetime," Nat. Methods **4**, 555–557 (2007).

22. J. Zhang, Y. Ma, S. S. Taylor, and R. Y. Tsien, "Genetically encoded reporters of protein kinase A activity reveal impact of substrate tethering," Proc. Nat. Acad. Sci. **98**, 14997–15002 (2001).
23. S. Scheuermann, B. Hambsch, L. Hesse, J. Stumm, C. Schmidt, D. Beher, T. A. Bayer, K. Beyreuther, and G. Multhaup, "Homodimerization of amyloid precursor protein and its implication in the amyloidogenic pathway of Alzheimer's disease," J. Biol. Chem. **276**, 33923–33929 (2001).
24. L. Jozefowski, J. Fiutowski, T. Kawalec, and H. G. Rubahn, "Direct measurement of the evanescent wave polarization state," J. Opt. Soc. Am. B **24**, 624–628 (2007).
25. M. Gee, L. Lensun, T. Smith, and C. Scholes, "Time-resolved evanescent wave-induced fluorescence anisotropy for the determination of molecular conformational changes of proteins at an interface," Eur. Biophys. J. **33**, 130–139 (2004).
26. K. Suhling, J. Siegel, P. Lanigan, S. Lévêque-Fort, S. Webb, D. Phillips, D. Davis, and P. French, "Time-resolved fluorescence anisotropy imaging applied to live cells," Opt. Lett. **29**, 584–586 (2004).
27. X. Michalet, F. F. Pinaud, L. A. Bentolila, J. M. Tsay, S. Doose, J. J. Li, G. Sundaresan, A. M. Wu, S. S. Gambhir, and S. Weiss, "Quantum dots for live cells, in vivo imaging, and diagnostics," Science **307**, 538–544 (2005).